NICST Internal Memo

Date: February 1, 2010
From: J. McIntire
To: Bruce Guenther, Jim Butler, and Jack Xiong
Subject: VIIRS F1 SI-4 TEB Radiometric Sensitivity to Electronic Cross Strapping (Cold and Hot Operational)

References:

[1] 'Command and Telemetry Verification, Test Procedure for (SI-4) – VIIRS,' TP154640-243_F.
[2] NICST_REPORT_09_031, 'VIIRS FU1 Cold Functional SI-4: Emissive Band Sensitivity to Cross-Strapping,' J. McIntire, June 5, 2009.
[3] NICST_REPORT_09_111, 'VIIRS FU1 SI-4: Emissive Band Sensitivity to Cross-Strapping,' J. McIntire, August 24, 2009.
[4] 'Sensor Performance Verification Plan (PVP) - VIIRS,' PVP154640-101_RevA-5.
[5] 'Performance Specification Sensor Specification,' ps154640-101_c.
[6] NICST_REPORT_09_038, 'RC-03 (TEB), P.2: Transition from Cold Operational to Cold Performance,' S. Marchenko and J. McIntire, June 11, 2009.
[7] NICST_REPORT_09_077, 'RC-03, P.4: FPA Cooldown at the Nominal Plateau,' S. Marchenko, July 16, 2009.

1. Introduction

SI-4 Part 2 was performed in part to assess VIIRS radiometric sensitivity to electronic cross strapping [1]. This work will focus on the TEB portion of this test. Of the eight possible power configurations available on VIIRS, four were tested during SI-4 (they are listed in Table 1). For the purposes of this work, the four configurations will be referred to as A, AX, B, and BX, where the A/B refers to the ASP/FPIE electronics and the X denotes cross-strapping in relation to the Spacecraft (S/C) Bus. This test was conducted at both Cold and Hot Operational Plateaus. The test data analyzed here is listed in Tables 1 and 2, along with the source temperatures and power configurations. This portion of SI-4 was performed in Diagnostic mode with the telescope rotating. Preliminary analysis for this work has been presented [2,3].

2. Data Analysis

This section describes the data processing. First, the SV DN is averaged over samples. Then, this sample averaged SV DN is subtracted from each sample of the EV DN. Next, the resulting EV dn is averaged first over samples and then over scans. This process is repeated for the OBC dn.

The EV and OBC dn for each power configuration are then compared to the A side configuration using a percent difference. These percent differences are then compared both within a given plateau as well as across plateaus.

In addition, the NEdT is compared across the four power configurations. The NEdT is computed by taking the scene radiance and dividing it by the SNR as well as the derivative of the Planck function evaluated at the scene radiance [4]. For those bands whose T_{TYP} is close to the BCS source temperature (I4, M12, and M14), the NEdT is compared to the specification as well [5].

3 Analysis Results

Figures 1 – 8 graph the percent differences of AX, B, and BX power configurations relative to A for the Cold Operational Plateau. Each figure contains two charts: the upper chart is the percent difference in EV dn and the lower chart is the percent difference in OBC dn. In both the EV and OBC dn, the AX configuration is roughly consistent with the A side configuration (all thermal bands). The BX and B configurations are consistent with each other but inconsistent with either the A or AX configuration (most thermal bands). The percent differences between the two groups are roughly: 0.5% for I4, I5, and M14; 2.0% for both M12 and M13; and 0.4% for both M16A and M16B. The exception is M15, where the four configurations are consistent to within 0.1%. In addition, note that vignetting occurs for detector 1 in all thermal bands (as noted in [6]).

The percent differences of AX, B, and BX power configurations relative to A for the Hot Operational Plateau are shown in Figures 9 – 16. Each figure contains two charts: the upper chart is the percent difference in EV dn and the lower chart is the percent difference in OBC dn. For the EV dn, the BX and B configurations are consistent with each other but inconsistent with either A or AX configurations (most thermal bands). The percent differences between the BX (or B) and A are roughly: 0.2% for I4, 0.5% for both I5 and M14; 2.0% for both M12 and M13; and 0.4% for both M16A and M16B. The exception is M15, where the A, BX, and B configurations are consistent to within 0.1%. This is in good agreement with the results from Cold Operational testing. For the MWIR, the AX configuration is in good agreement with A; in contrast, the AX configuration is between 1.5% and 3.0% different from A for the LWIR. This is the probable result of a change in LWIR CFPA temperature for this collect. Figure 17 plots the LWIR CFPA temperature for both Cold and Hot Operational Plateaus (upper and lower charts). Each collect is denoted by a different color. The last collect (AX configuration) at the Hot Operational Plateau has a LWIR CFPA temperature ~1 K larger than the other collects. From RC-03 Part 4 results [7], the LWIR bands vary between 2 – 4% per degree K.

For the lower charts in Figures 9 – 16, the percent difference in OBC dn is graphed. However, the OBC temperature is not constant for the Hot Operational Plateau. Figure 18 shows the OBC temperature for both Cold and Hot Operational Plateaus (upper and lower charts). Each collects is denoted by a different color. The OBC temperature is constant for the Cold Operational Plateau, but changes by 0.2 – 0.3 K per collect for the Hot Operational Plateau. For the LWIR, the percent difference in OBC dn of BX and B relative to A is small (less than 0.5%), but the percent difference of AX relative to A is 2.0 - 3.0%. This is roughly in agreement with the results of Cold Operational testing when the change in CFPA temperature is taken into account. For the MWIR, the percent difference in OBC dn of BX and B relative to A is 1.0 – 4.0%, and the percent difference of AX relative to A is about 3.0%. The sensitivity of the MWIR to CFPA temperature changes is minimal [7]. The gains for these bands are much larger than for the LWIR; as a result, the same increase in OBC temperature causes a larger increase in the dn, which in turn results in a greater percent difference. However, for M12 and M13, the AX configuration has a smaller percent difference from A than BX or B, yet corresponds to a larger OBC temperature. This results because, under a constant source temperature the percent differences of BX and B relative to A are about 2.0% (see the case of the EV dn at Cold Operational); this offsets the percent differences in OBC dn at Hot Operational for M12 and M13 and as a result, the percent difference of AX is smaller than that of BX or B relative to A.

The ratio of the EV dn to the OBC dn for both Cold and Hot Operational plateaus (upper and lower graphs, respectively) is shown in Figures 19 – 26 for all thermal bands. For the Cold Operational results, the variation of the dn ratio is small (less than 0.002 for all bands and detectors). Also, note that the ratio for detector 1 is not consistent with the other detectors; this is the result of vignetting for detector 1 for all bands at very low instrument temperatures [6]. For the Hot Operational results, the dn ratio slightly decreases with collect for all bands. This corresponds to a slight increase (0.2 – 0.3 K) in OBC temperature and consequent increase in OBC dn, while the EV dn remains roughly constant.

The NEdT for each band is shown in Figures 27 – 34; the upper and lower charts plot the NEdT for the Cold and Hot Operational Plateaus, respectively. For all bands the NEdT is consistent across power configurations and shows a slight increase from Cold to Hot Operational. In addition, T_{TYP} for I4, M12, and M14 corresponds roughly to the BCS temperature; as a result, the NEdT for these bands is compared to the specification SRV0053 (the red horizontal line in each plot). All detectors in I4, M12, and M14 meet the specification.

4. Summary

- Change in S/C power side has a minimal impact; in contrast, changes in the ASP/FPIE side causes variation in dn of roughly 0.5% for I4, I5, and M14, 2.0% for both M12 and M13, and 0.4% for both M16A and M16B. [A side configuration is consistent with AX for all bands; B side is configuration consistent with BX for all bands.]
- NEdT is consistent over power configuration and slightly increases over plateau; bands I4, M12, and M14 were measured at T_{TYP} and so compared to the specification SRV0053, which all detectors pass.
- Vignetting is observed in detector 1 for all bands during Cold Operational Plateau (but not during Hot Operational Plateau). Cold Operational Plateau is well below normal operating conditions on-orbit.

Acknowledgement

The sensor test data used in this document was provided by the SBRS testing team. Approaches for data acquisition and data reductions, as well as data extraction tools were also provided by the SBRS. We would like to thank the SBRS team for their support. The data analysis tools were developed by the NICST team, and we would like to extend our gratitude for their valued assistance.

Table 1: VIIRS F1 SI-4 power configurations

UAID	Plateau	Collect	Configuration	ASP/FPIE	1394 Bus	Servo Elec	Proc Chain	S/C Power
U3103292	Cold	10	A	A	A	A	A	A
U3103293	Cold	9	BX	B	B	B	B	A
U3103294	Cold	9	AX	A	A	A	A	B
U3102295	Cold	9	B	B	B	B	B	B
U3104522	Hot	9	A	A	A	A	A	A
U3104523	Hot	9	BX	B	B	B	B	A
U3104524	Hot	9	B	B	B	B	B	B
U3104525	Hot	9	AX	A	A	A	A	B

Table 2: VIIRS F1 SI-4 source temperatures

UAID	Plateau	Collect	T_bcs (K)	T_obc (K)
U3103292	Cold	10	269.9	292.6
U3103293	Cold	9	269.9	292.6
U3103294	Cold	9	269.9	292.6
U3102295	Cold	9	269.9	292.6
U3104522	Hot	9	270.0	293.7
U3104523	Hot	9	270.0	293.9
U3104524	Hot	9	270.0	294.1
U3104525	Hot	9	270.0	294.3

Figure 1: Percent differences in I4 EV and OBC dn for Cold Operational Plateau

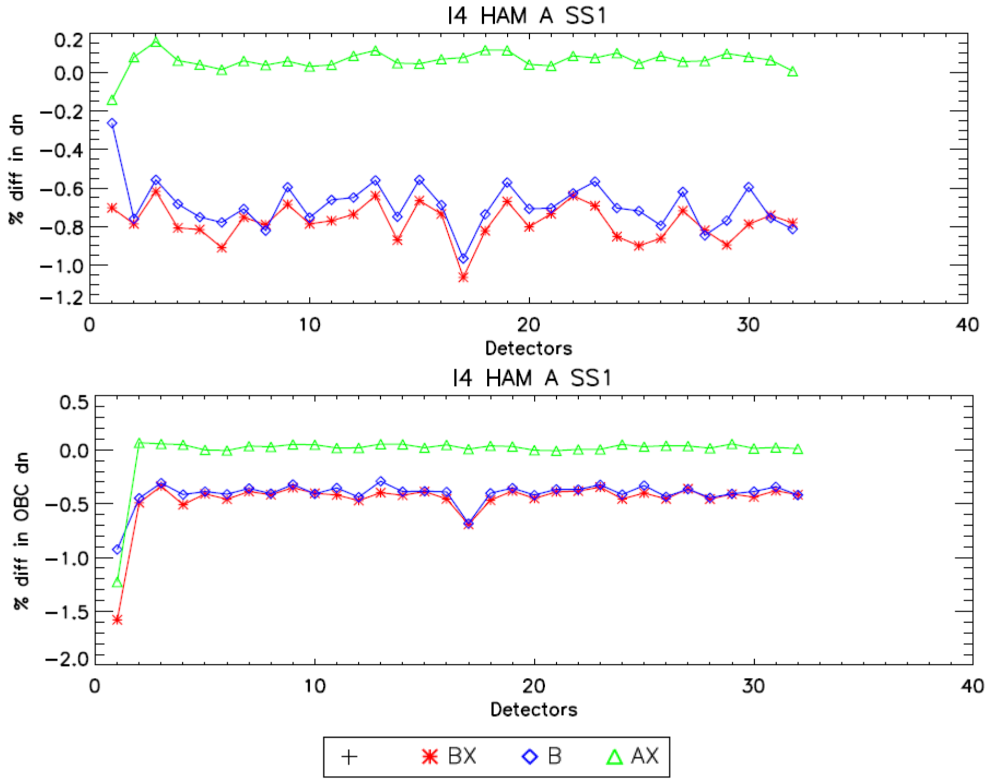

Figure 2: Percent differences in I5 EV and OBC dn for Cold Operational Plateau

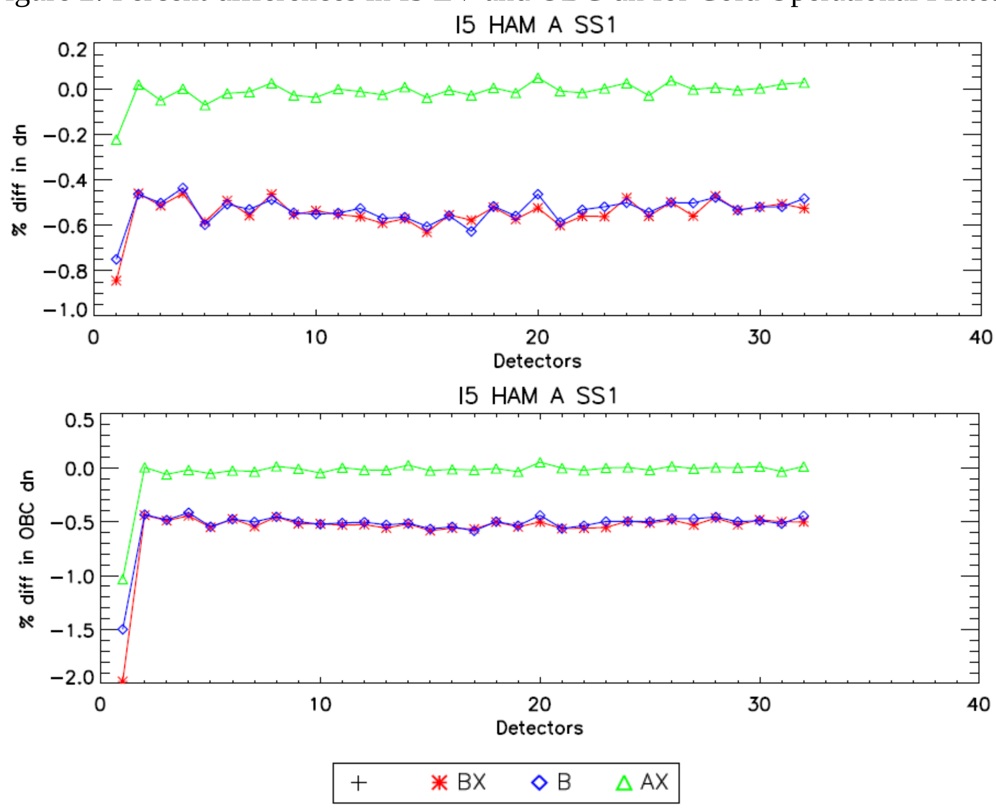

Figure 3: Percent differences in M12 EV and OBC dn for Cold Operational Plateau

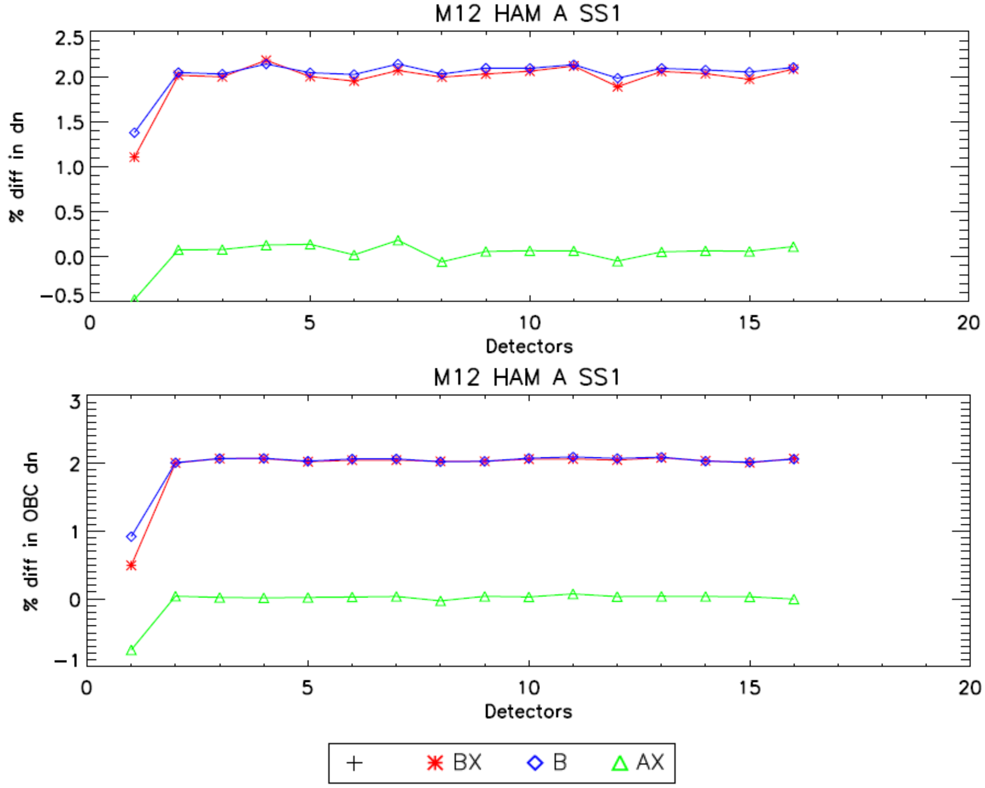

Figure 4: Percent differences in M13 EV and OBC dn for Cold Operational Plateau

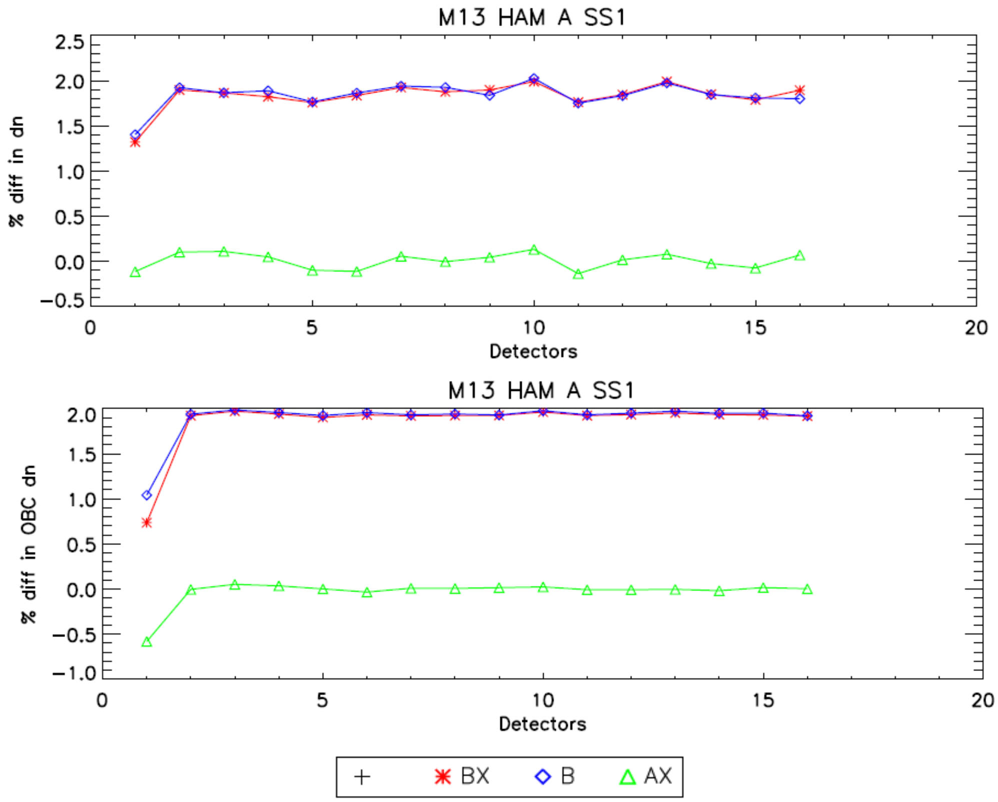

Figure 5: Percent differences in M14 EV and OBC dn for Cold Operational Plateau

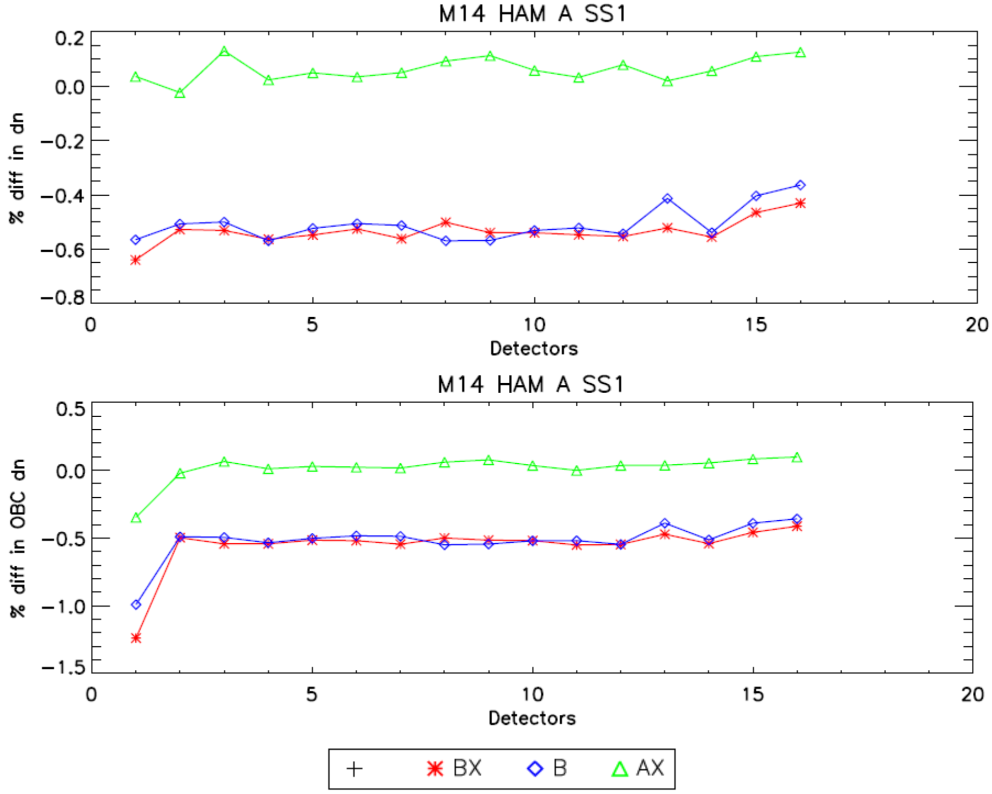

Figure 6: Percent differences in M15 EV and OBC dn for Cold Operational Plateau

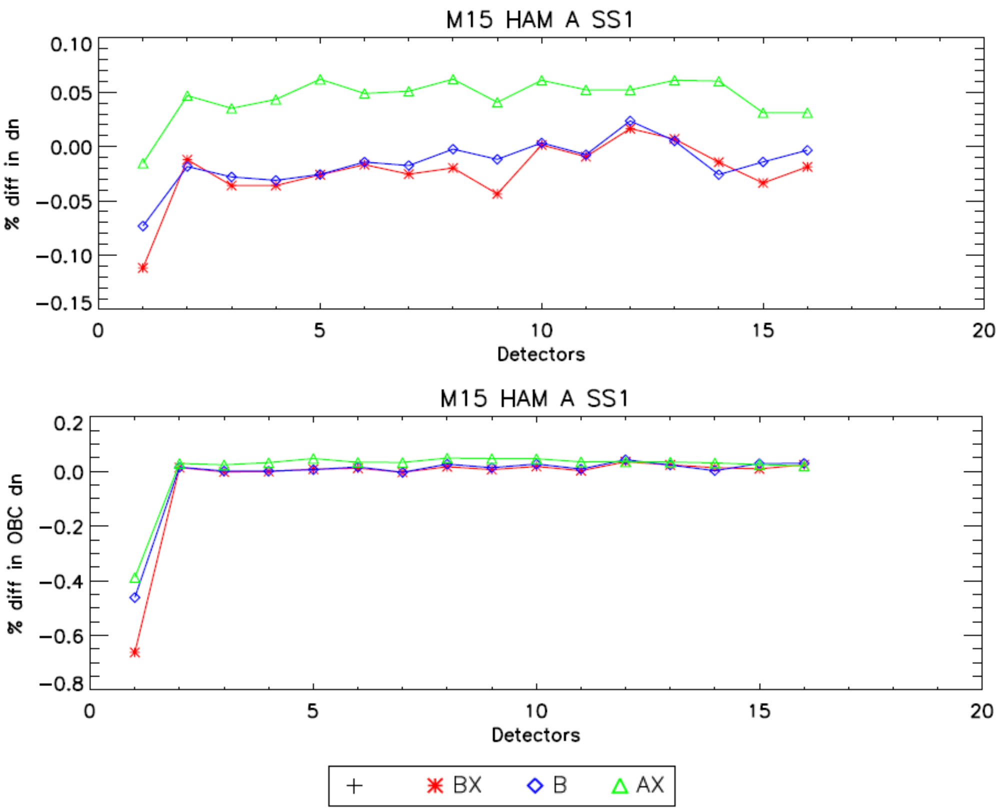

Figure 7: Percent differences in M16A EV and OBC dn for Cold Operational Plateau

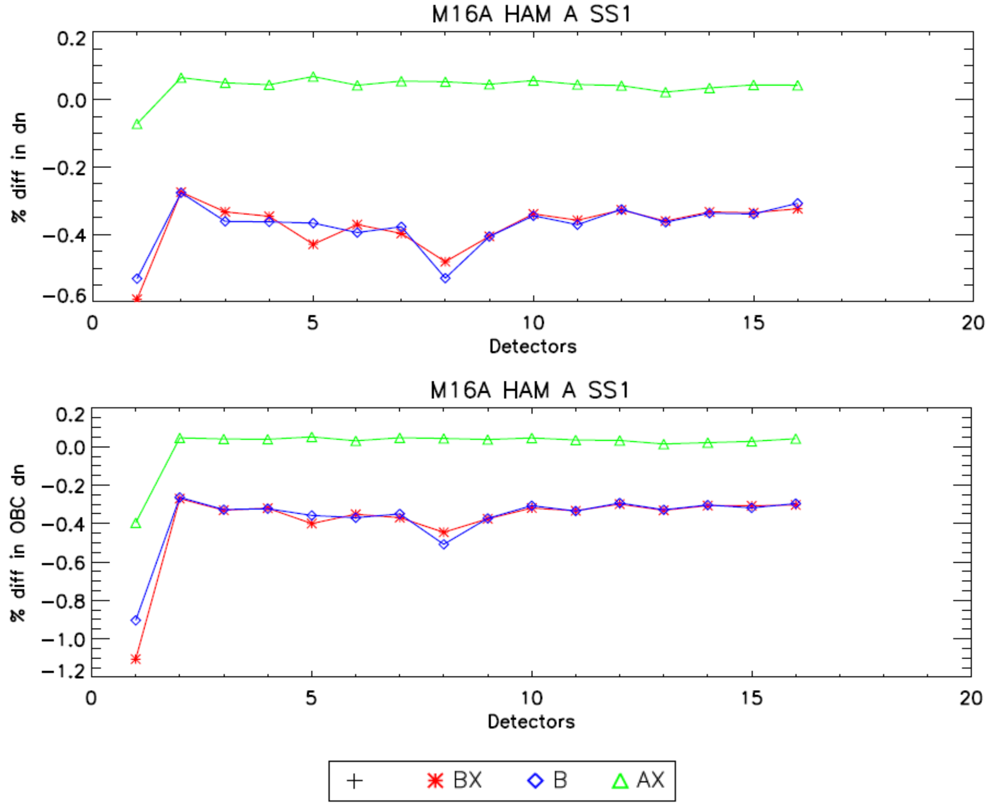

Figure 8: Percent differences in M16B EV and OBC dn for Cold Operational Plateau

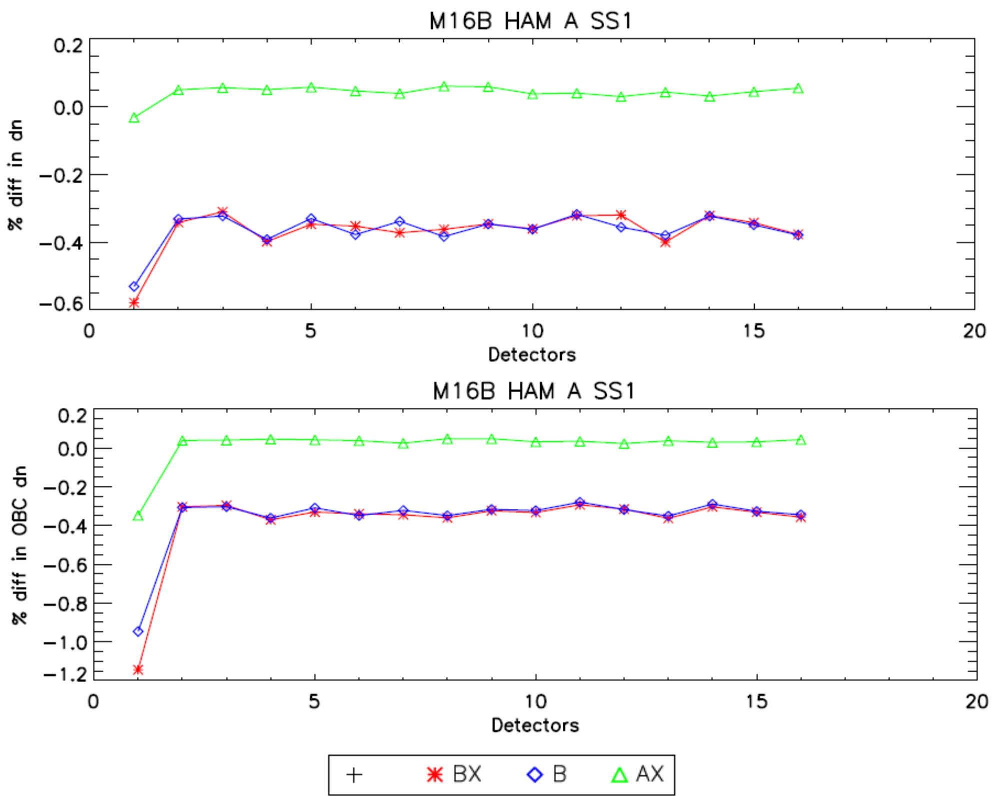

Figure 9: Percent differences in I4 EV and OBC dn for Hot Operational Plateau

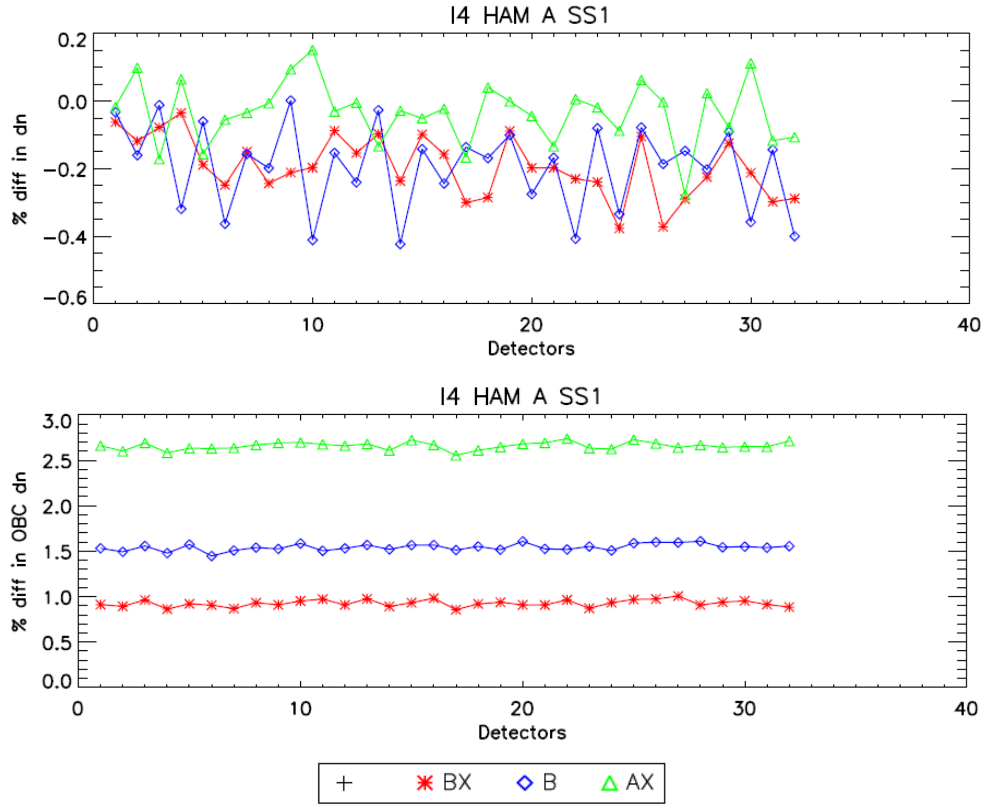

Figure 10: Percent differences in I5 EV and OBC dn for Hot Operational Plateau

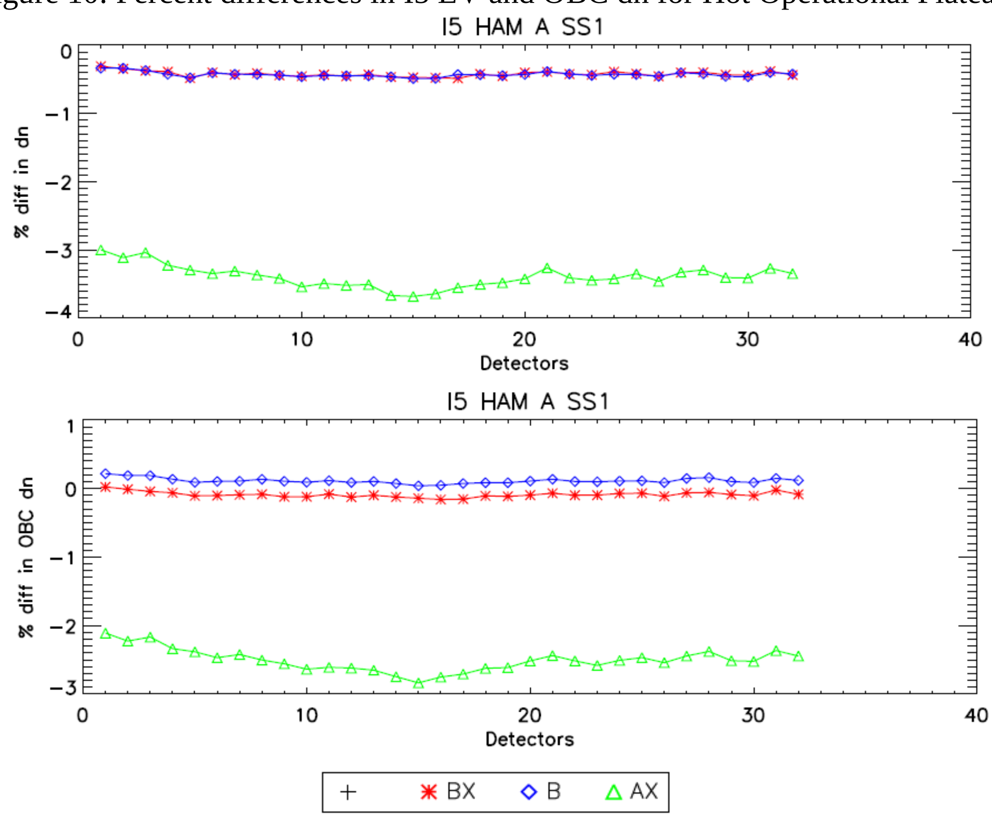

Figure 11: Percent differences in M12 EV and OBC dn for Hot Operational Plateau

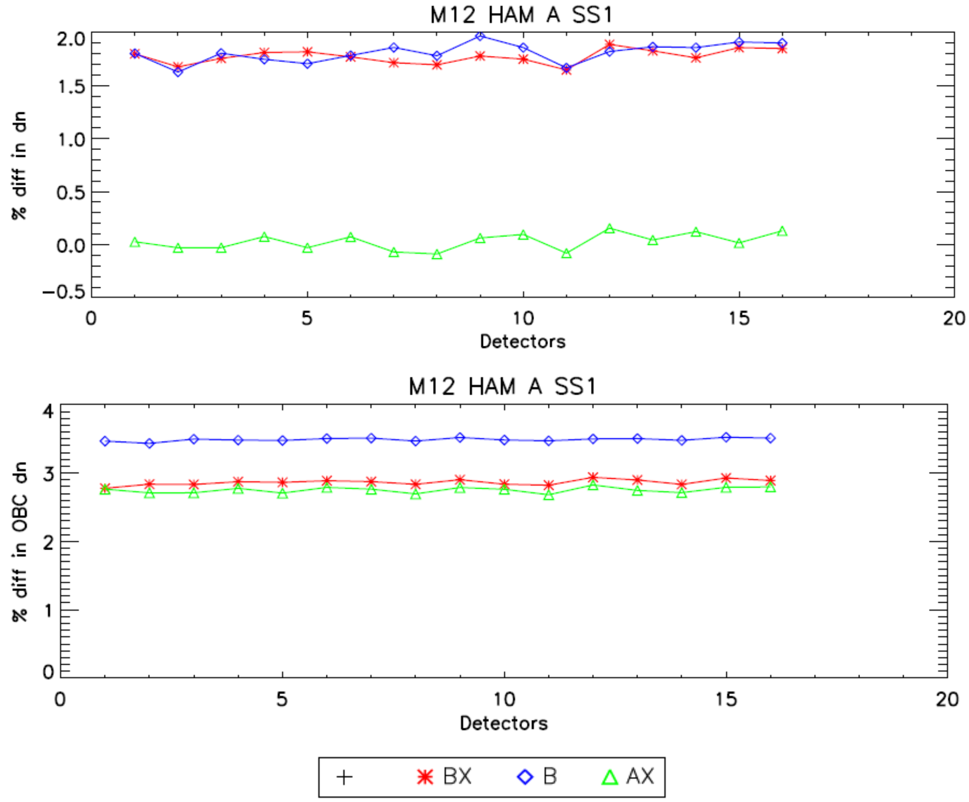

Figure 12: Percent differences in M13 EV and OBC dn for Hot Operational Plateau

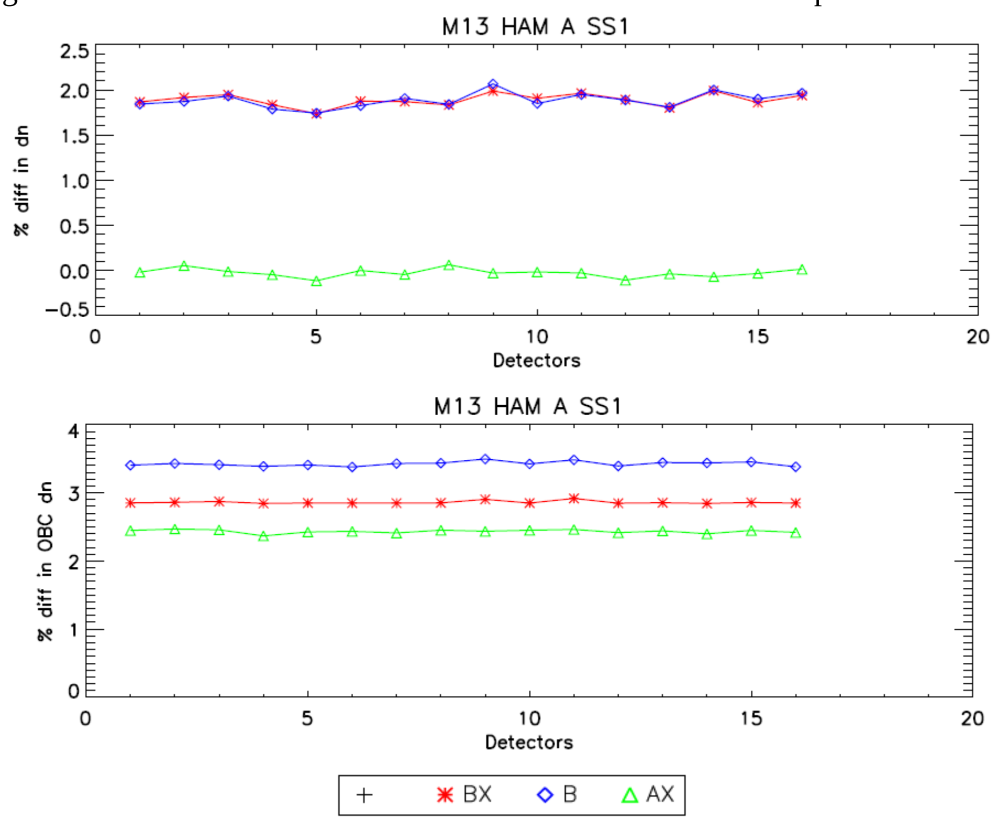

Figure 13: Percent differences in M14 EV and OBC dn for Hot Operational Plateau

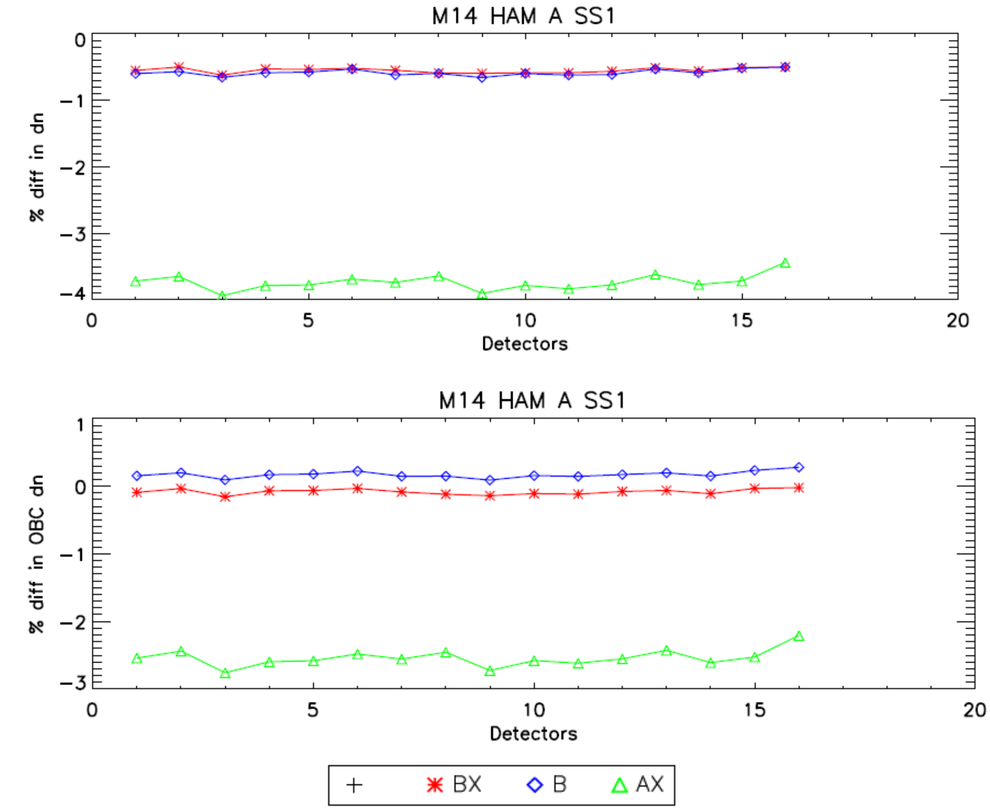

Figure 14: Percent differences in M15 EV and OBC dn for Hot Operational Plateau

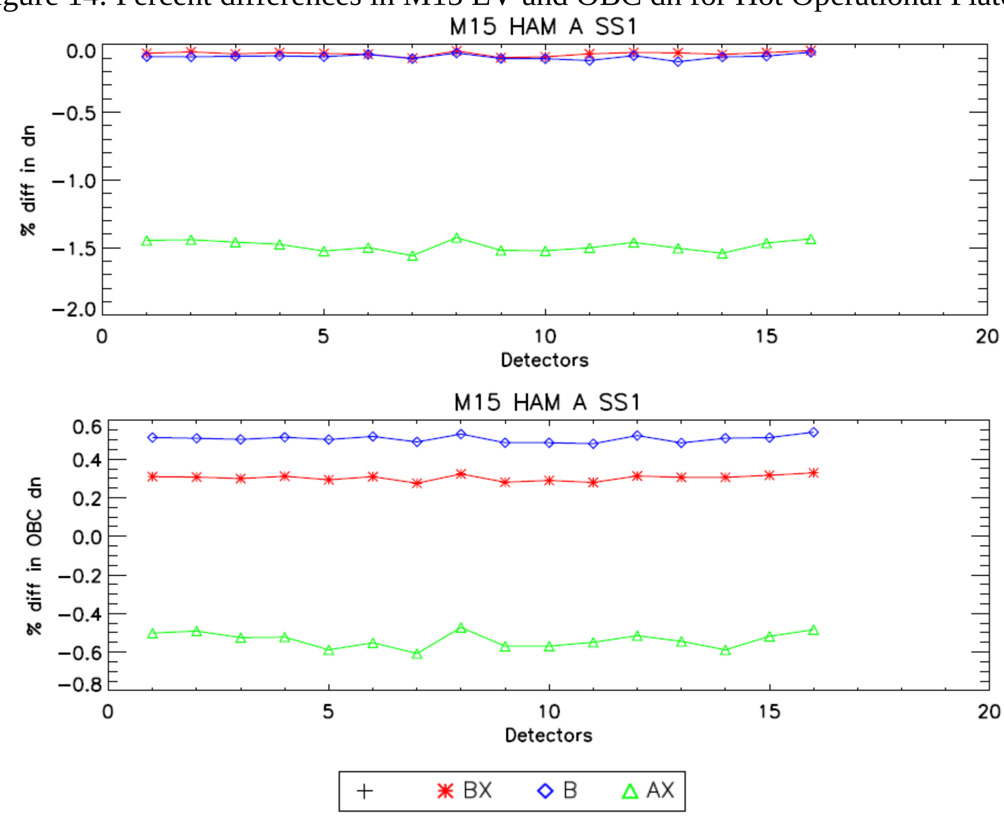

Figure 15: Percent differences in M16A EV and OBC dn for Hot Operational Plateau

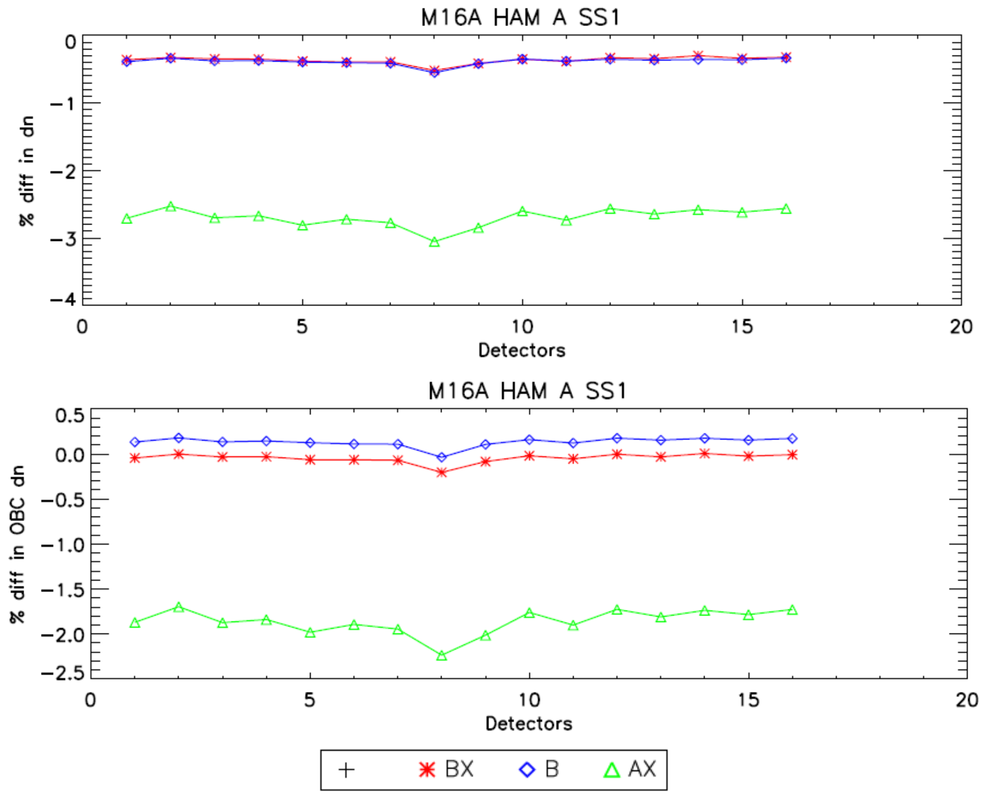

Figure 16: Percent differences in M16B EV and OBC dn for Hot Operational Plateau

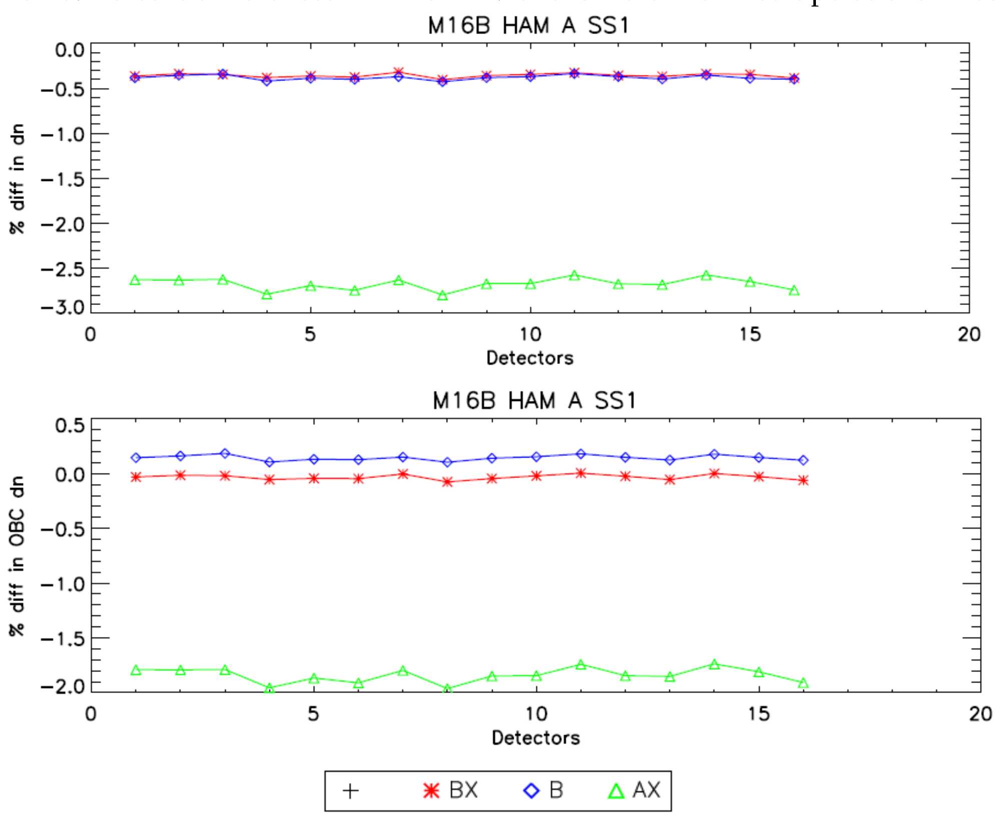

Figure 17: SI-4 LWIR CFPA temperature for Cold and Hot Operational Plateaus

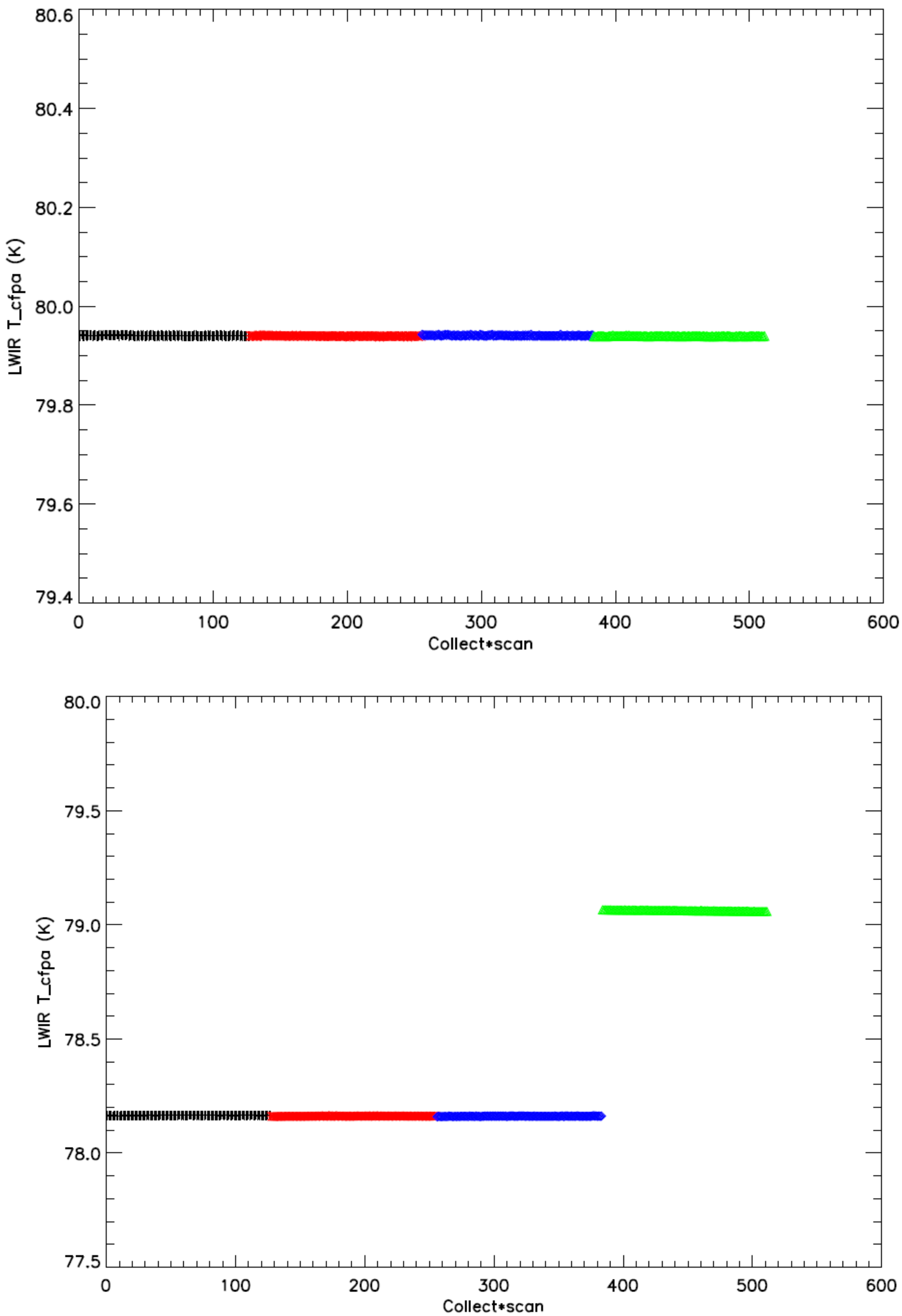

Figure 18: SI-4 OBC temperature for Cold and Hot Operational Plateaus

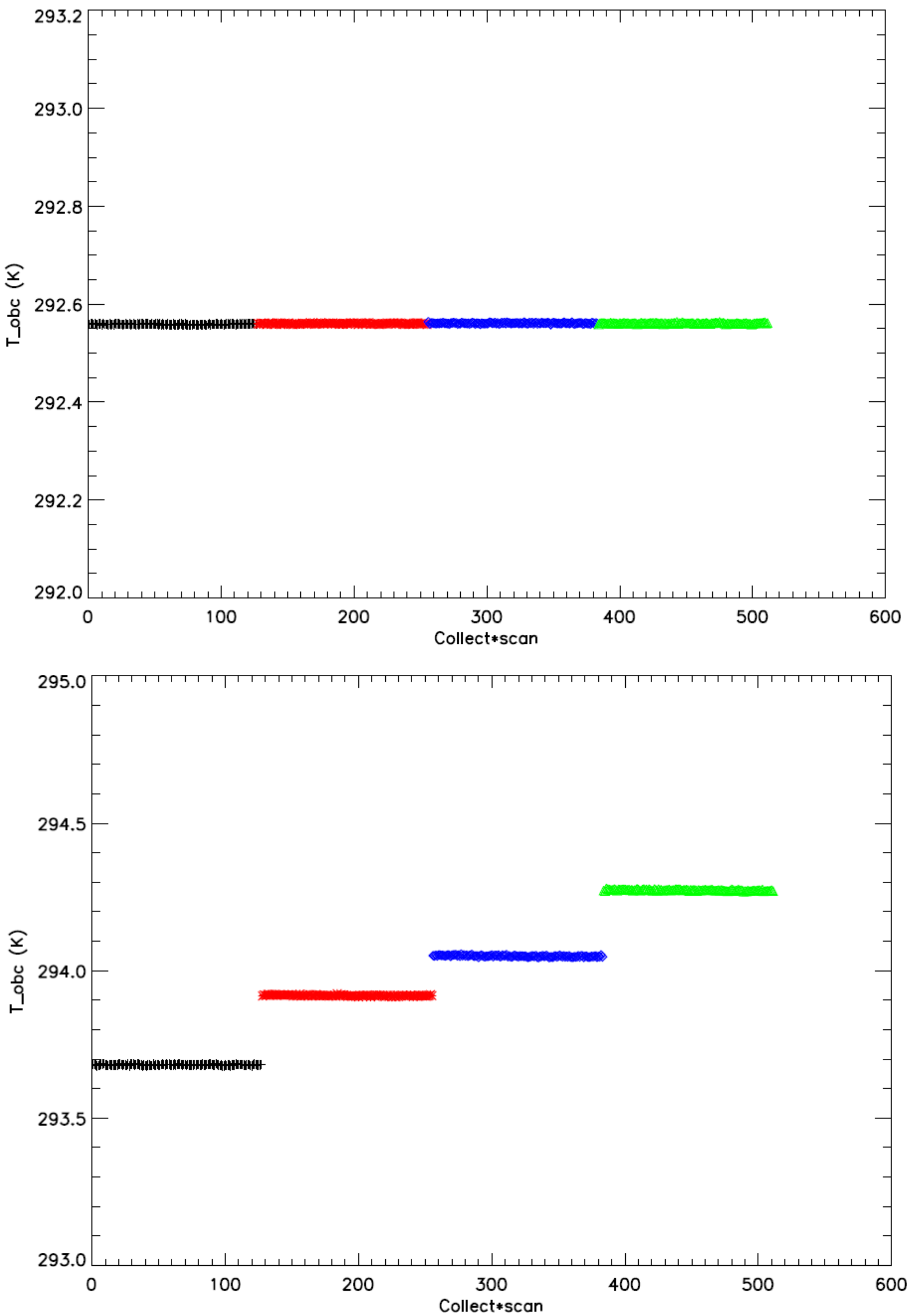

Figure 19: Ratio of I4 EV to OBC dn for both Cold and Hot Operational Plateaus

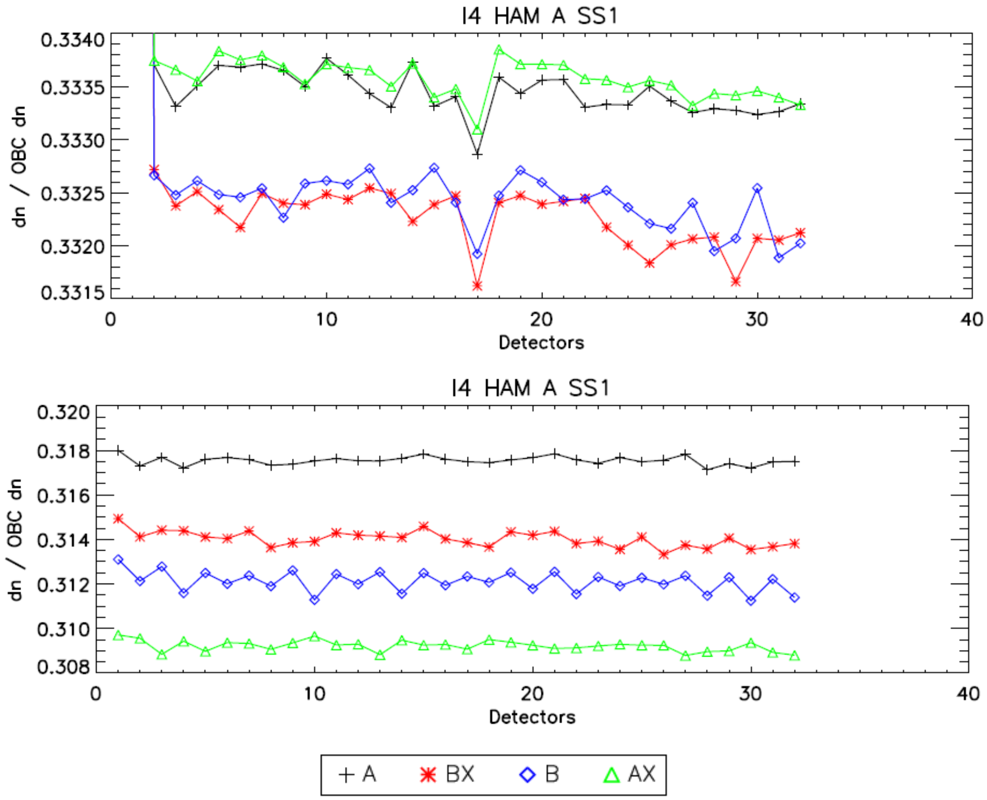

Figure 20: Ratio of I5 EV to OBC dn for both Cold and Hot Operational Plateaus

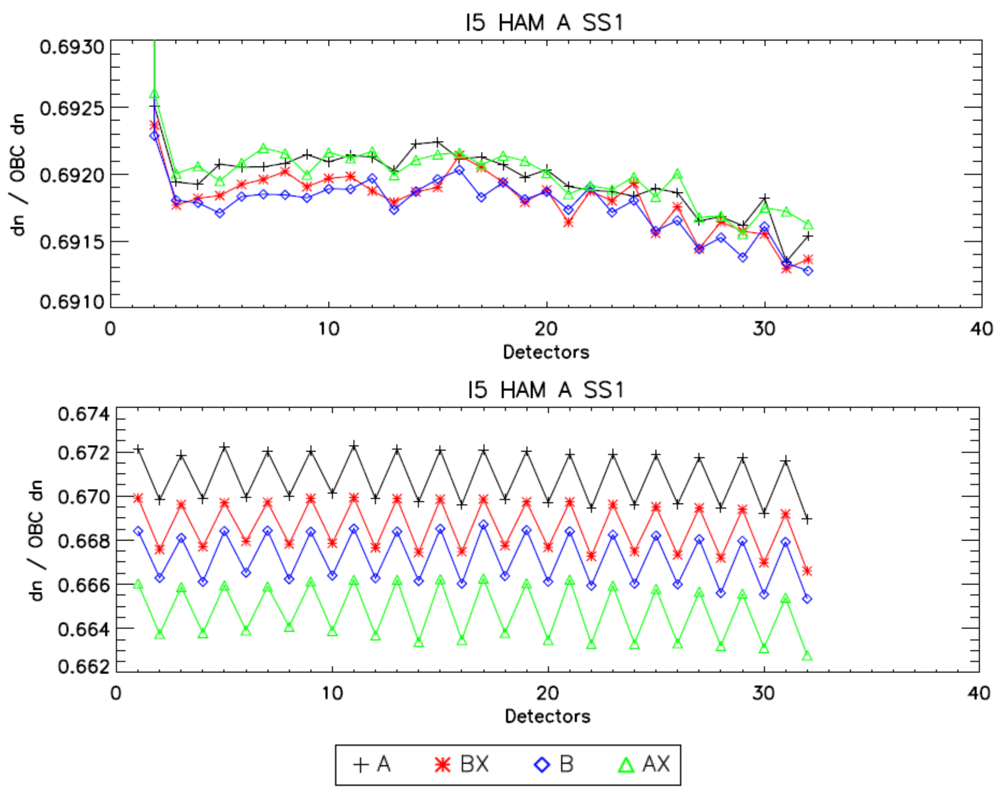

Figure 21: Ratio of M12 EV to OBC dn for both Cold and Hot Operational Plateaus

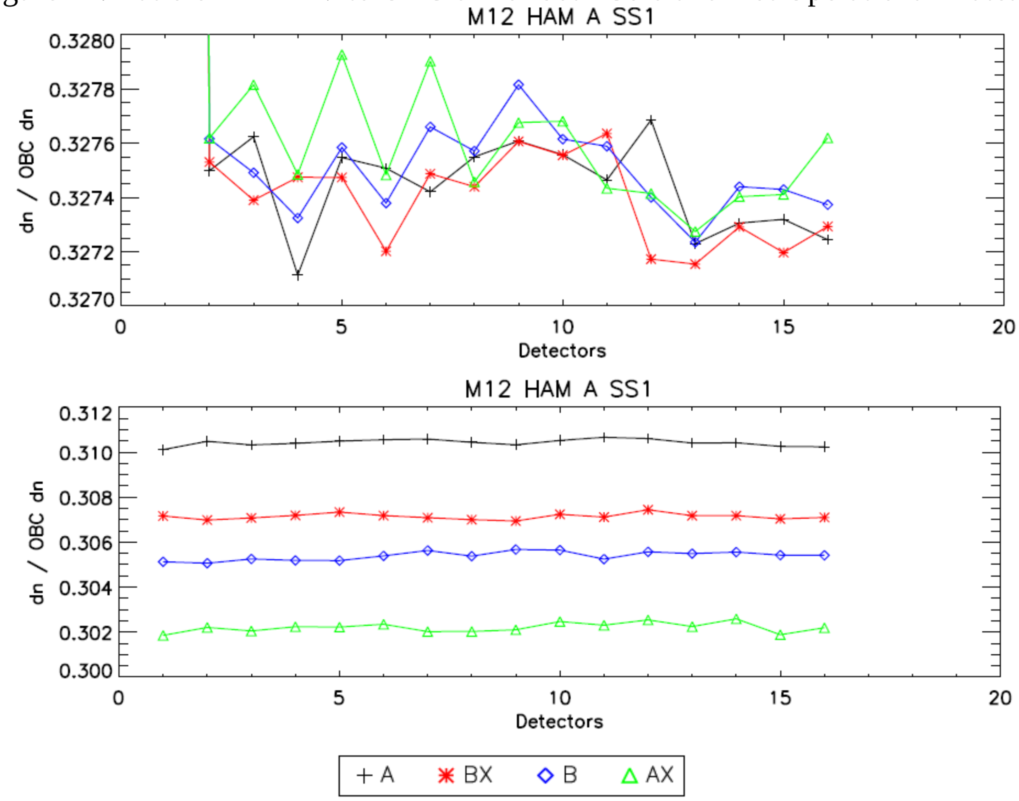

Figure 22: Ratio of M13 EV to OBC dn for both Cold and Hot Operational Plateaus

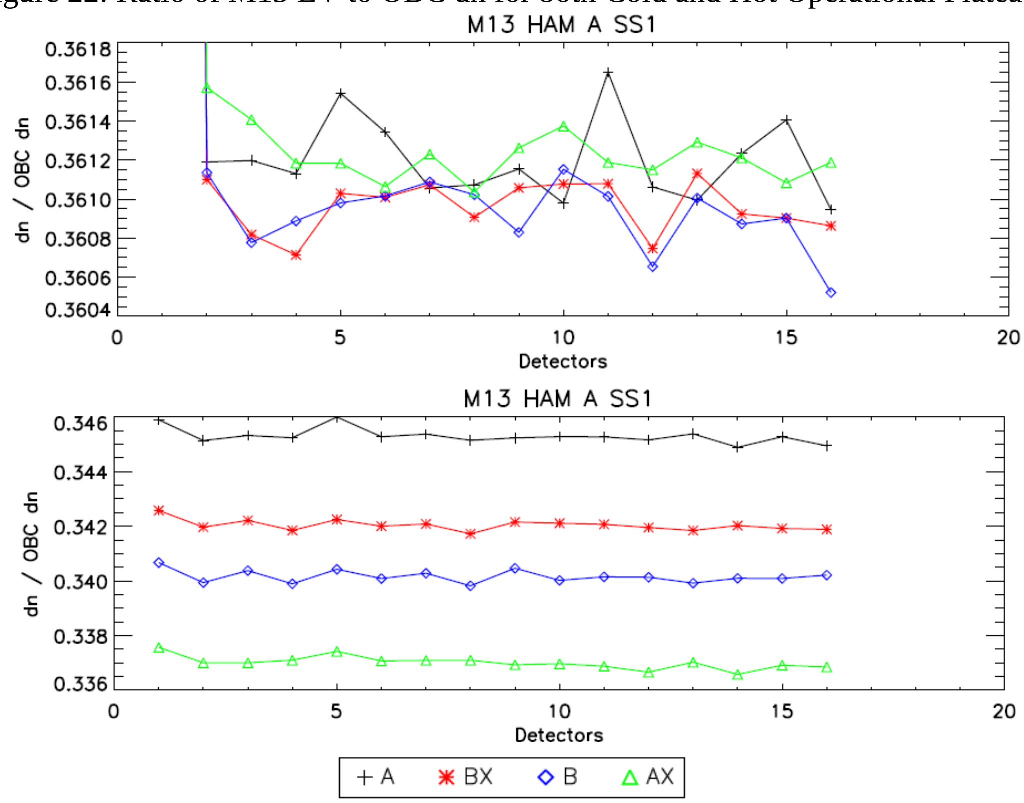

Figure 23: Ratio of M14 EV to OBC dn for both Cold and Hot Operational Plateaus

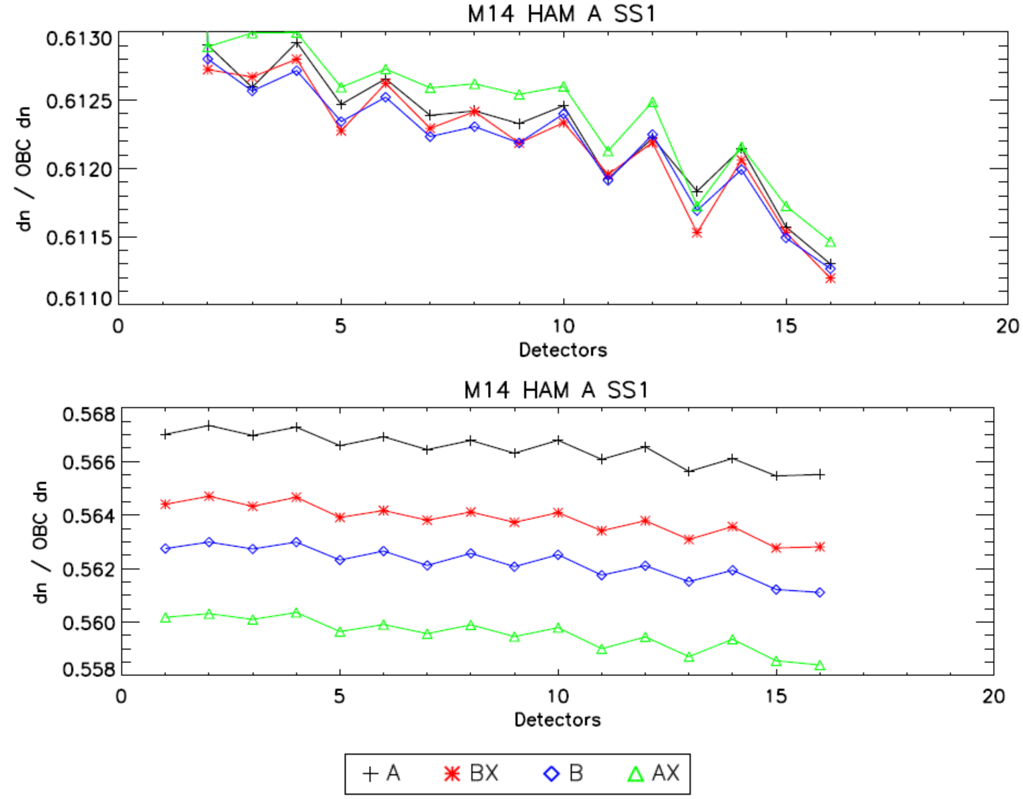

Figure 24: Ratio of M15 EV to OBC dn for both Cold and Hot Operational Plateaus

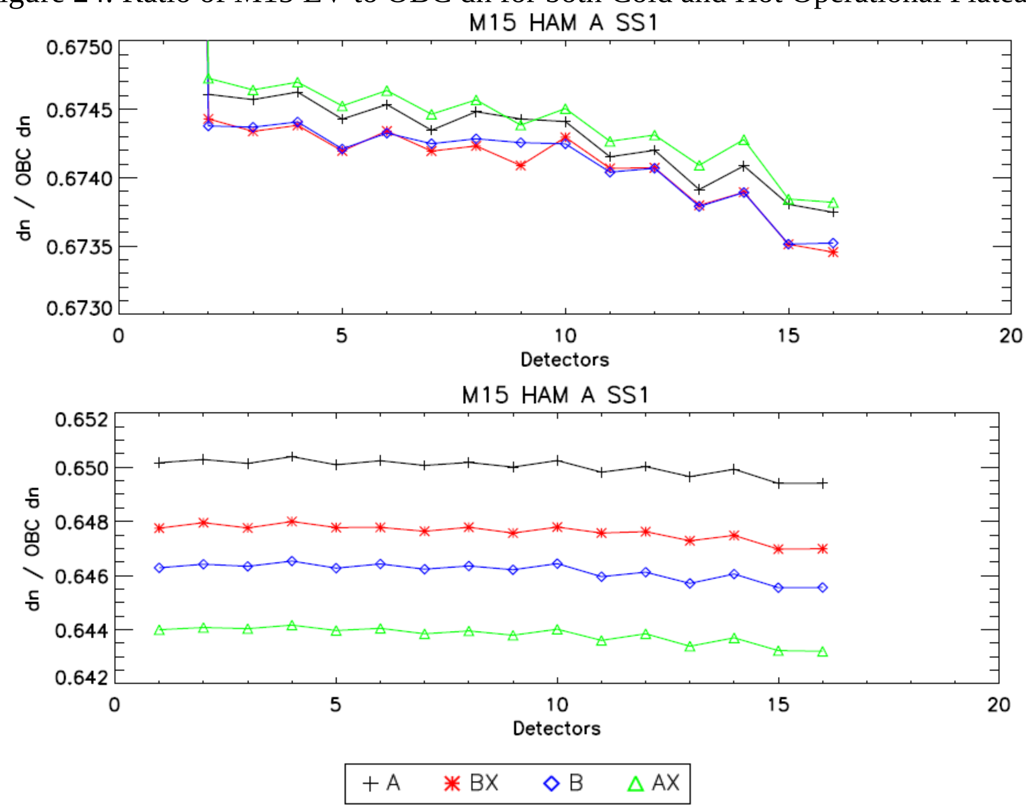

Figure 25: Ratio of M16A EV to OBC dn for both Cold and Hot Operational Plateaus

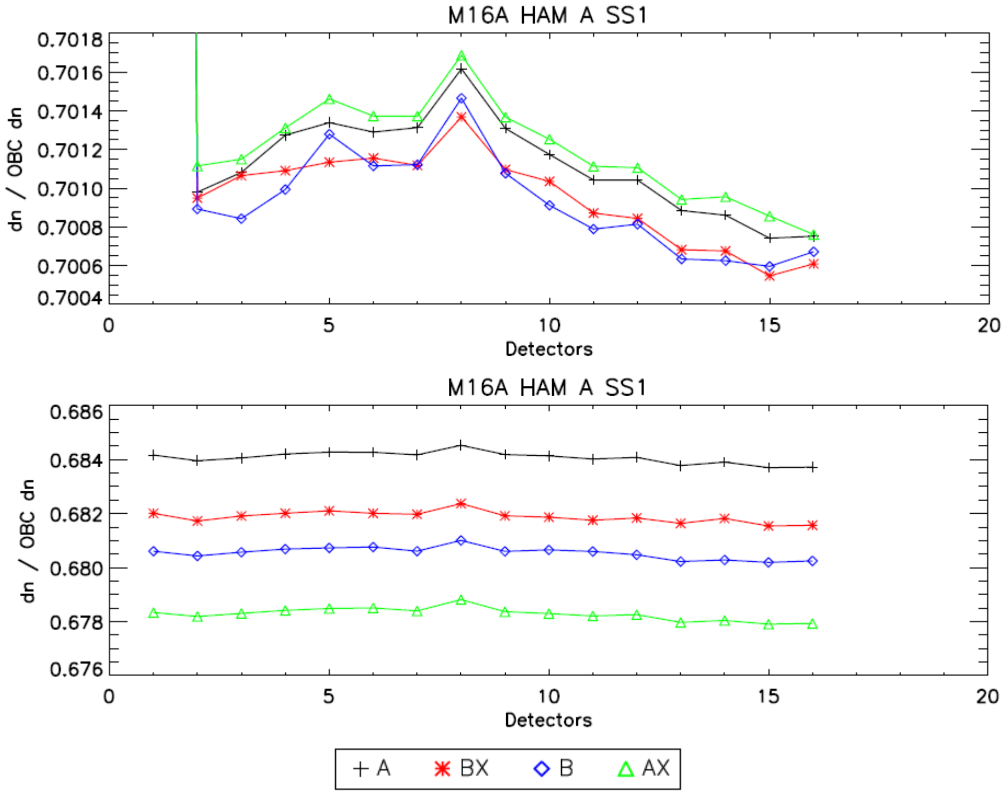

Figure 26: Ratio of M16B EV to OBC dn for both Cold and Hot Operational Plateaus

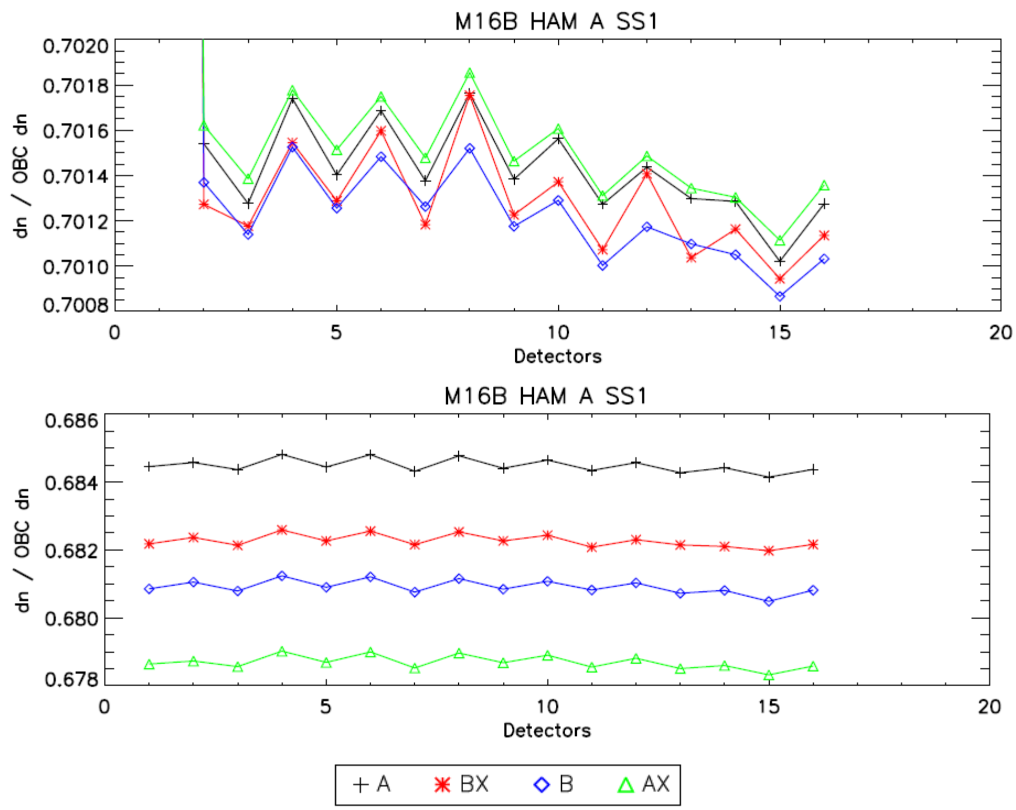

Figure 27: I4 EV NEdT from both Cold and Hot Operational Plateaus

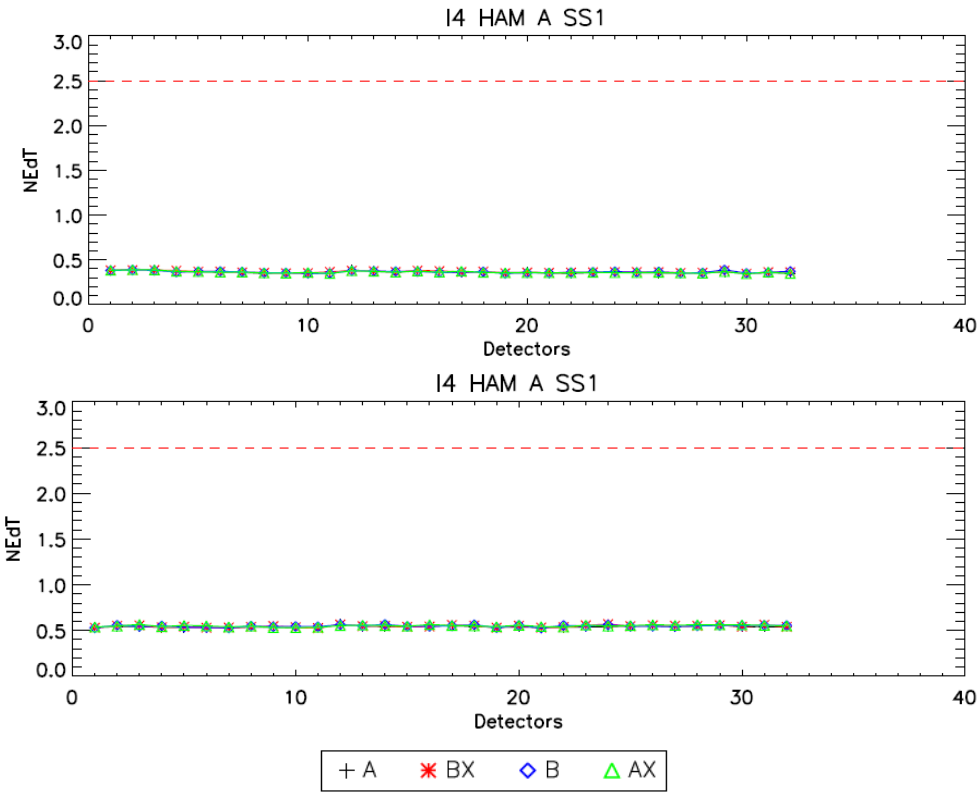

Figure 28: I5 EV NEdT from both Cold and Hot Operational Plateaus

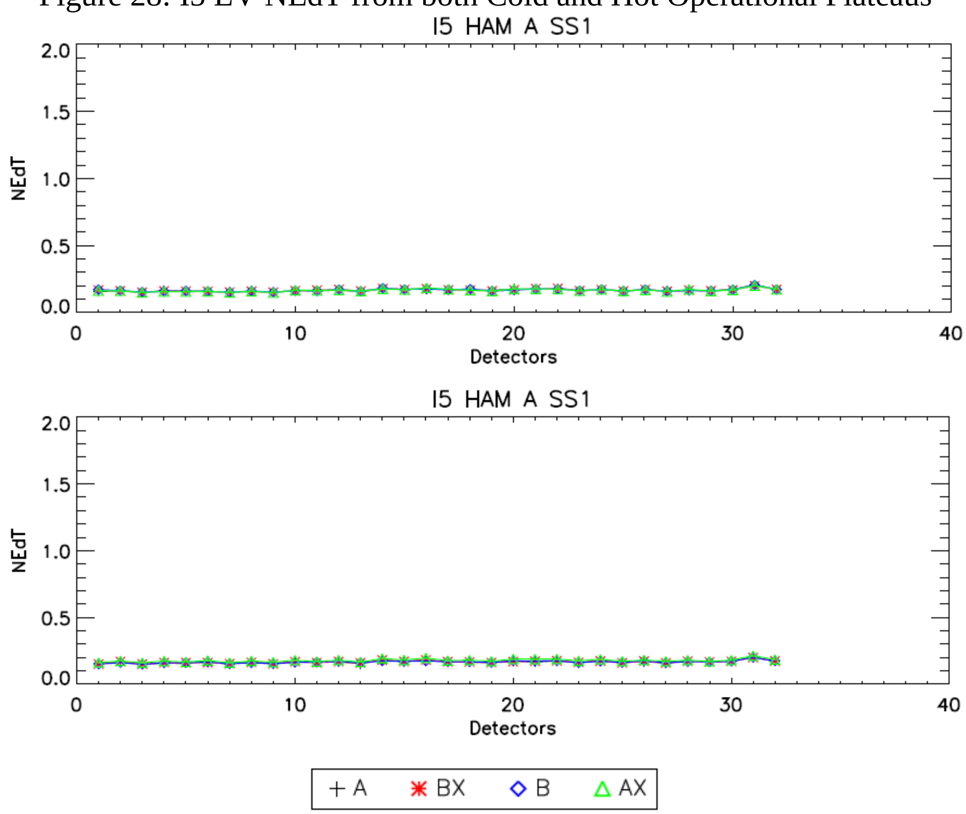

Figure 29: M12 EV NEdT from both Cold and Hot Operational Plateaus

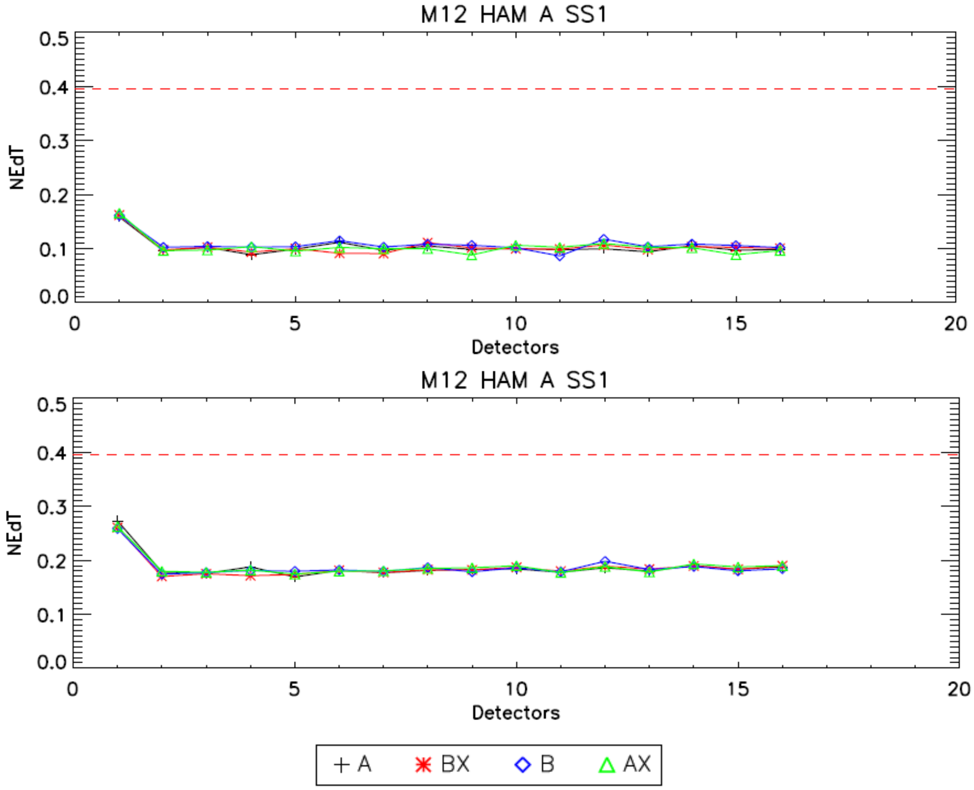

Figure 30: M13 EV NEdT from both Cold and Hot Operational Plateaus

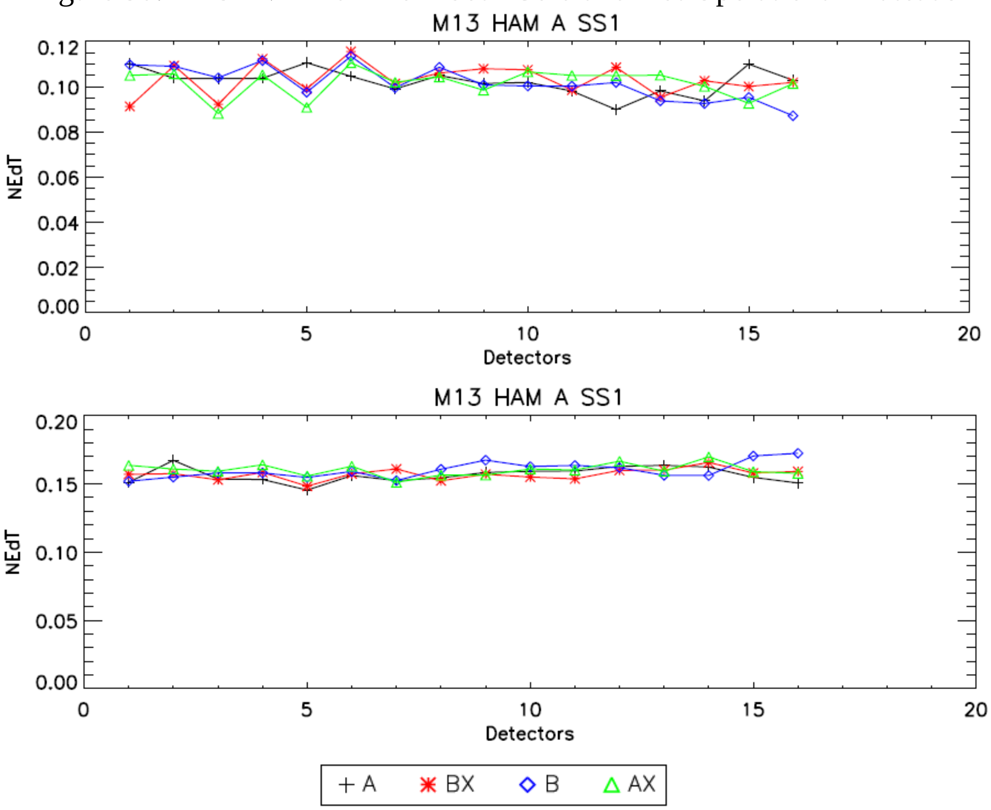

Figure 31: M14 EV NEdT from both Cold and Hot Operational Plateaus

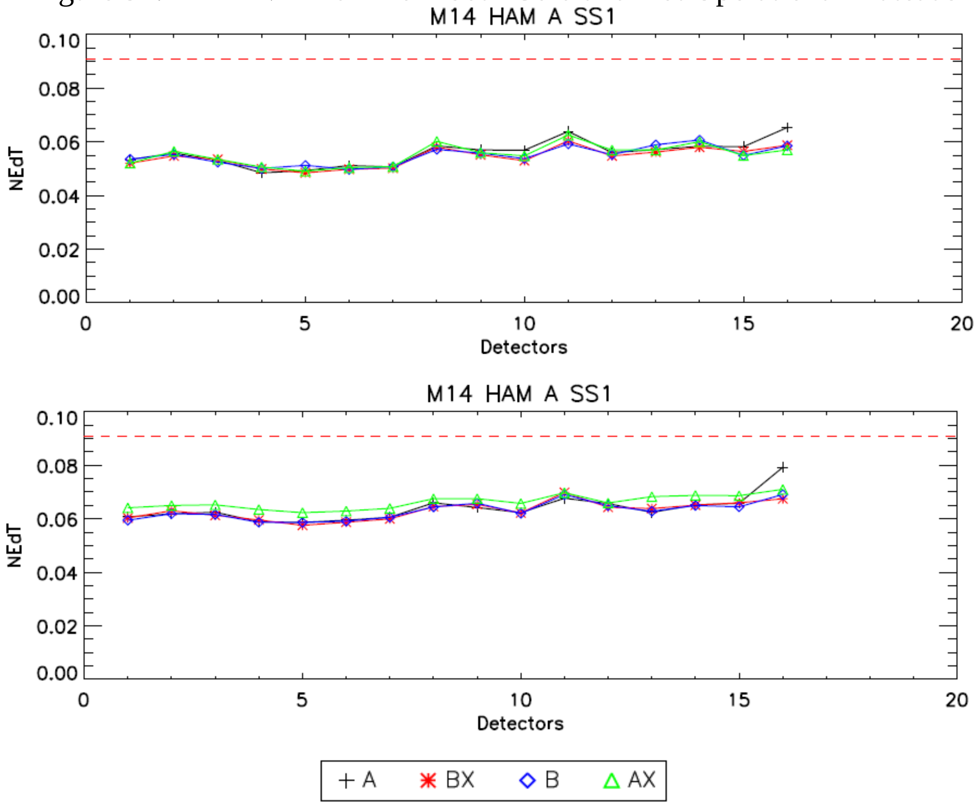

Figure 32: M15 EV NEdT from both Cold and Hot Operational Plateaus

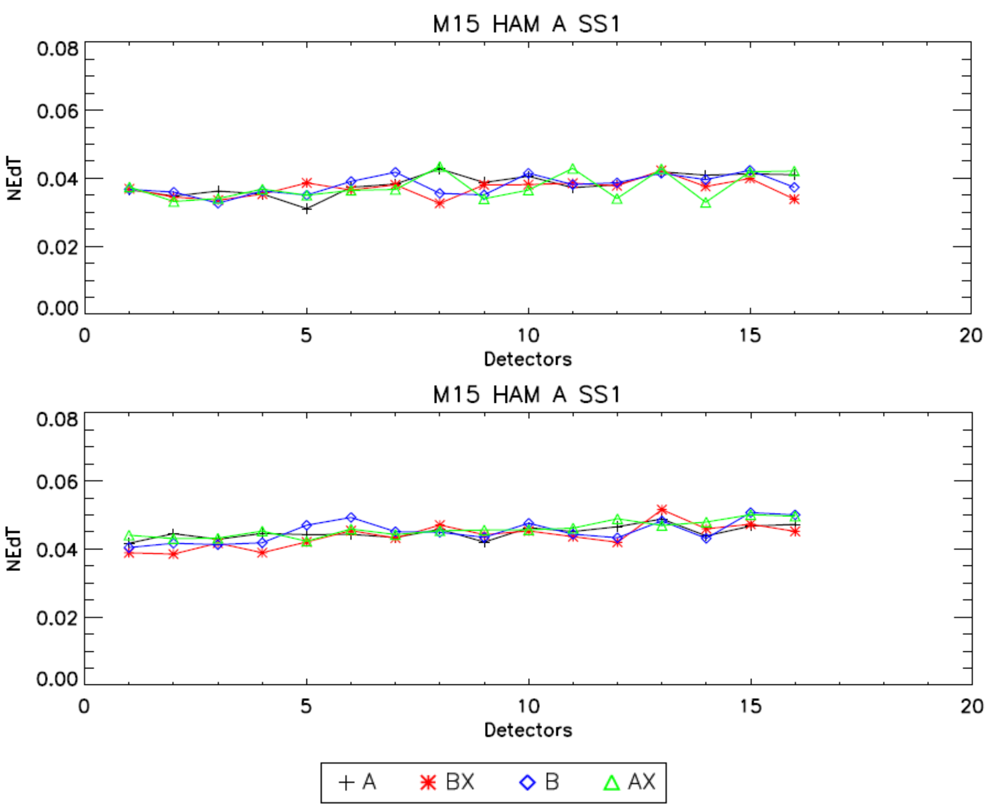

Figure 33: M16A EV NEdT from both Cold and Hot Operational Plateaus

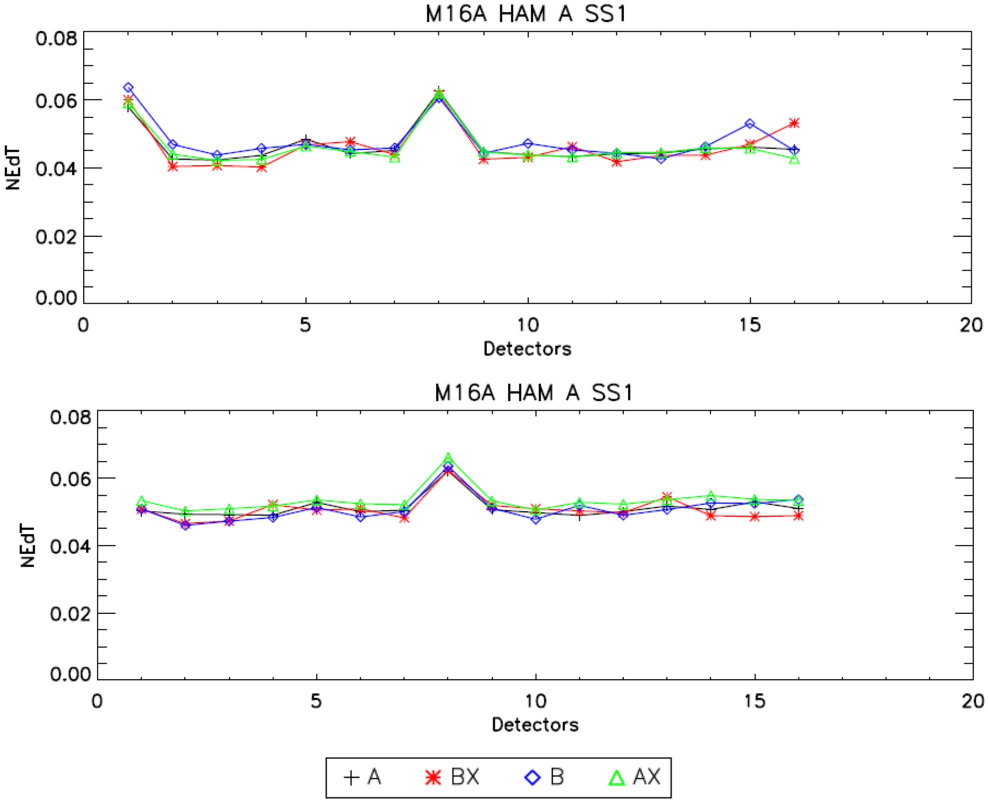

Figure 34: M16B EV NEdT from both Cold and Hot Operational Plateaus